



## Atmospheric events disrupting coastal upwelling in the southwestern Caribbean

Serguei A. Lonin,<sup>1</sup> José L. Hernández,<sup>2</sup> and Daniel M. Palacios<sup>3,4</sup>

Received 28 August 2008; revised 11 December 2009; accepted 11 January 2010; published 30 June 2010.

[1] Year-round coastal upwelling is a prevalent phenomenon in the southwestern Caribbean region, driven by northeast trade winds. This pattern can be disrupted during the boreal winter-to-spring transition by event-scale departures in the pressure systems, characterized by a change in wind direction to northward, with the accompanying relaxation of coastal upwelling. To study these poorly understood events, regional atmospheric and data-assimilative ocean modeling experiments were carried out for the period 4 March to 9 April 2003 and compared to shipboard observations. This combined ocean-atmosphere approach allowed us to study the evolution of a 3-day atmospheric disturbance affecting ocean currents and collapsing the upwelling pattern against the Colombian coast along the Guajira Peninsula near 12°N. The southward extension of the coastal upwelling, which normally reaches 10.5°N, was blocked by the warmer and slightly lower salinity waters of the cyclonic Panama-Colombia gyre. Under typical conditions, the ocean model and shipboard observations of temperature and salinity profiles were in good agreement with each other, both at coastal and oceanic stations. The presence of a low-level westward wind jet was manifested in the atmospheric model simulation, confirming that it promotes the Guajira upwelling system; however, the jet vanishes under disturbed atmospheric conditions.

**Citation:** Lonin, S. A., J. L. Hernández, and D. M. Palacios (2010), Atmospheric events disrupting coastal upwelling in the southwestern Caribbean, *J. Geophys. Res.*, 115, C06030, doi:10.1029/2008JC005100.

### 1. Introduction

[2] Coastal upwelling in the southwestern Caribbean is a well-known process driven by northeast trade winds running parallel to the northern coast of South America. While the process has been studied from the ocean perspective [Richards, 1960; Gordon, 1967; Corredor, 1979; Müller-Karger and Aparicio, 1994; Andrade and Barton, 2005], coupled numerical experiments can provide a more complete description by considering ocean-atmosphere-land interactive processes. The diverse physiographic features in the region (coastline orientation, topography, and land cover) influence the land-air-sea exchanges of properties and exert control over surface level pressure and winds, thus affecting the local to regional coastal processes, like upwelling.

[3] Early investigations of the dynamics of the Caribbean Sea reported upwelling and elevated primary production

along the coast of Venezuela [Richards, 1960] and the Guajira Peninsula in Colombia [Curl, 1960]. Gordon [1967] evaluated geostrophic velocities and transport in the region and provided the first estimate of upwelling in the Colombian Basin at 74°W ( $\sim 4 \times 10^{-4}$  cm/s at the base of the Ekman layer). In the same region, Corredor [1979] found that shallow inshore areas (above 30 m) receive upwelled nutrients that stimulate phytoplankton growth. More recently, Müller-Karger and Aparicio [1994] examined the surface temporal and spatial variability of coastal upwelling centers in the southern Caribbean, including the northeastern Colombian region, where a combination of local coastal upwelling and advection from the Gulf of Venezuela can lead to very large patches of high phytoplankton pigment concentrations. According to Andrade and Barton [2005], the Caribbean low-level wind jet [Vernekar et al., 2003] maintains the strong upwelling close to the coast at the Guajira Peninsula. This coastal upwelling interacts with Caribbean circulation patterns in such a way that it is limited in its northward extent to 13°N by the main Caribbean Current and in its westward extent to about 75°W by the warmer waters of the Panama-Colombia Countercurrent [Carton and Chao, 1999; Oey et al., 2003; Centurioni and Niiler, 2003; Foltz et al., 2004; Richardson, 2005].

[4] Disruptions to coastal upwelling are linked to changes in wind speed and direction [Hawkins and Stuart, 1980; Enriquez and Friehe, 1995]. In the western Caribbean, equatorward atmospheric departures originating at the mid

<sup>1</sup>Facultad de Oceanografía Física, Escuela Naval de Cadetes “Almirante Padilla,” Cartagena, Colombia.

<sup>2</sup>Agricultural and Biological Engineering Department, University of Florida, Gainesville, Florida, USA.

<sup>3</sup>Joint Institute for Marine and Atmospheric Research, University of Hawaii, Hilo, Hawaii, USA.

<sup>4</sup>Environmental Research Division, Southwest Fisheries Science Center, National Oceanic and Atmospheric Administration, Pacific Grove, California, USA.

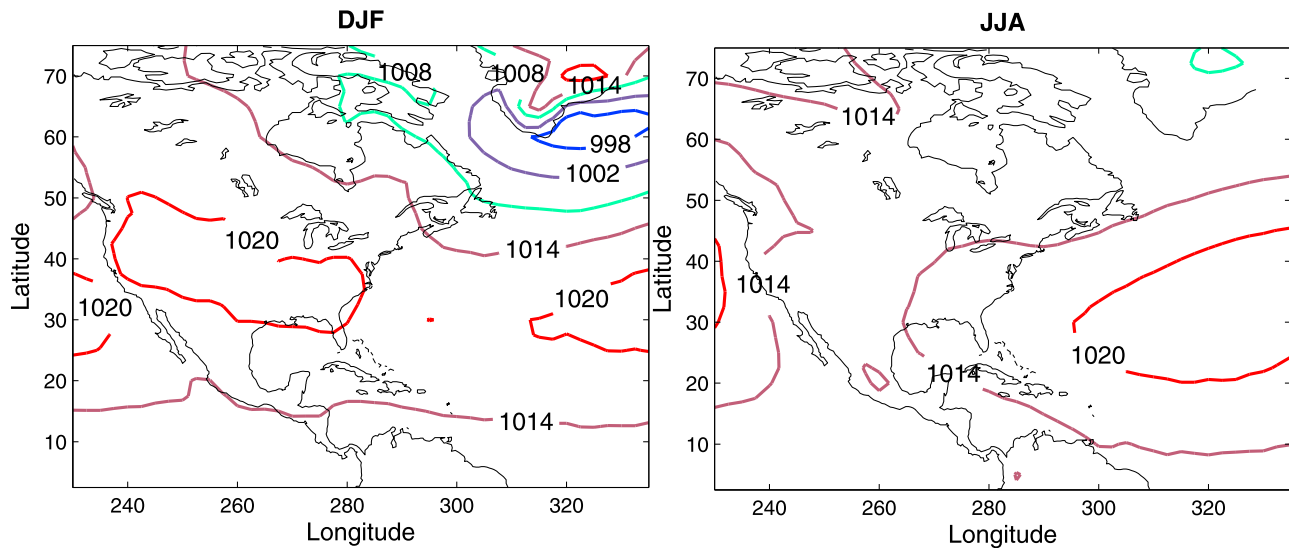


**Figure 1.** 1978–2008 seasonal climatology of SLP from NCEP/NCAR reanalysis. This plot shows high and low SLP systems in winter and summer. The Azores and Canadian highs and the Iceland Low are main pressure systems in the region.

northern latitudes can abruptly change the normal wind pattern, bringing cold surges lasting less than a week as far south as the Isthmus of Panama [Shultz *et al.*, 1998]. Less known are events associated with surface winds flowing poleward from the southwestern Caribbean, transporting warm air northward, and reaching southern North America. Since both types of events take place at the same time of the year, around mid-March, they are likely connected to an annual transition in the location of the semipermanent high- and low-pressure systems and to pressure changes over the continent.

[5] In the present study, we report on the evolution of an event of the latter type based on a combination of ocean and atmosphere modeling experiments for the period 4 March to 9 April 2003. We use an ocean model that assimilates satellite-derived sea surface temperature while simultaneously nudging salinity to the climatological state. Measurements from an oceanographic cruise during 26–30 March 2003 are considered for model evaluation. We also use a mesoscale atmospheric model in a nested domain configuration to gain further insight into the regional forcing of the Caribbean Basin and its relationship to the large-scale atmospheric pressure systems that drive the regional patterns. In this case, we use sea level pressure (SLP) observations as an independent set for model evaluation.

## 2. Study Region

[6] The Colombian Basin is a region subject to the interaction of large-scale, mesoscale, and local scale ocean-atmosphere-land processes. Climatologically, the configuration of the regional surface pressure systems at the beginning of the year consists of high pressure in the Atlantic (Azores High) and over the continent (Canadian High), the Intertropical Convergence Zone (ITCZ) located south of the equator, and the Iceland Low at higher latitudes in the North Atlantic. The Canadian High disappears in summer, being replaced by a low-pressure system over the

continent, while the ITCZ moves northward, the Azores High extends over the mid-Atlantic, and the Icelandic Low weakens. Figure 1 presents the 30 year climatological distribution of SLP in winter (December–February) and in summer (June–August) from the National Centers for Environmental Prediction (NCEP)/National Center for Atmospheric Research (NCAR) reanalysis [Kalnay *et al.*, 1996], illustrating the main pressure systems in the region described above. During the winter-spring transition, around mid-March, abrupt changes in wind direction take place over the tropics, when cold air is still pushing from polar regions while warm air begins to invade from lower latitudes. At this time, the continental topography between the Pacific and Atlantic basins has a role in controlling the transport of humidity and in pushing the ITCZ southward on the Pacific side [Xu *et al.*, 2005].

[7] The region under scrutiny in this work is depicted in Figure 2, which shows part of the Colombian Basin, the location of oceanographic stations during a 2003 cruise, and the bathymetry and topography of the region. The cruise stations cover the shelf off the Colombian Guajira Peninsula, where winds parallel to the coast promote strong upwelling throughout the year. A relative shallow coastal area (<400 m) extends 40–70 km off the western shoreline followed by a steep continental slope that reaches 4000 m at some 200 km off the peninsula. On land, a coastal plain is characteristic of the region, only being interrupted by the Sierra Nevada de Santa Marta, the world’s highest coastal mountain, reaching 5775 m above sea level just 42 km from the coast.

## 3. Methods

[8] Our analyses consist of modeling experiments supported by observational data. In situ measurements were taken from 26 to 30 March 2003 by the Caribe 2003 oceanographic cruise on board R/V *Malpelo*, conducted by the Centro de Investigaciones Oceanográficas e Hidro-

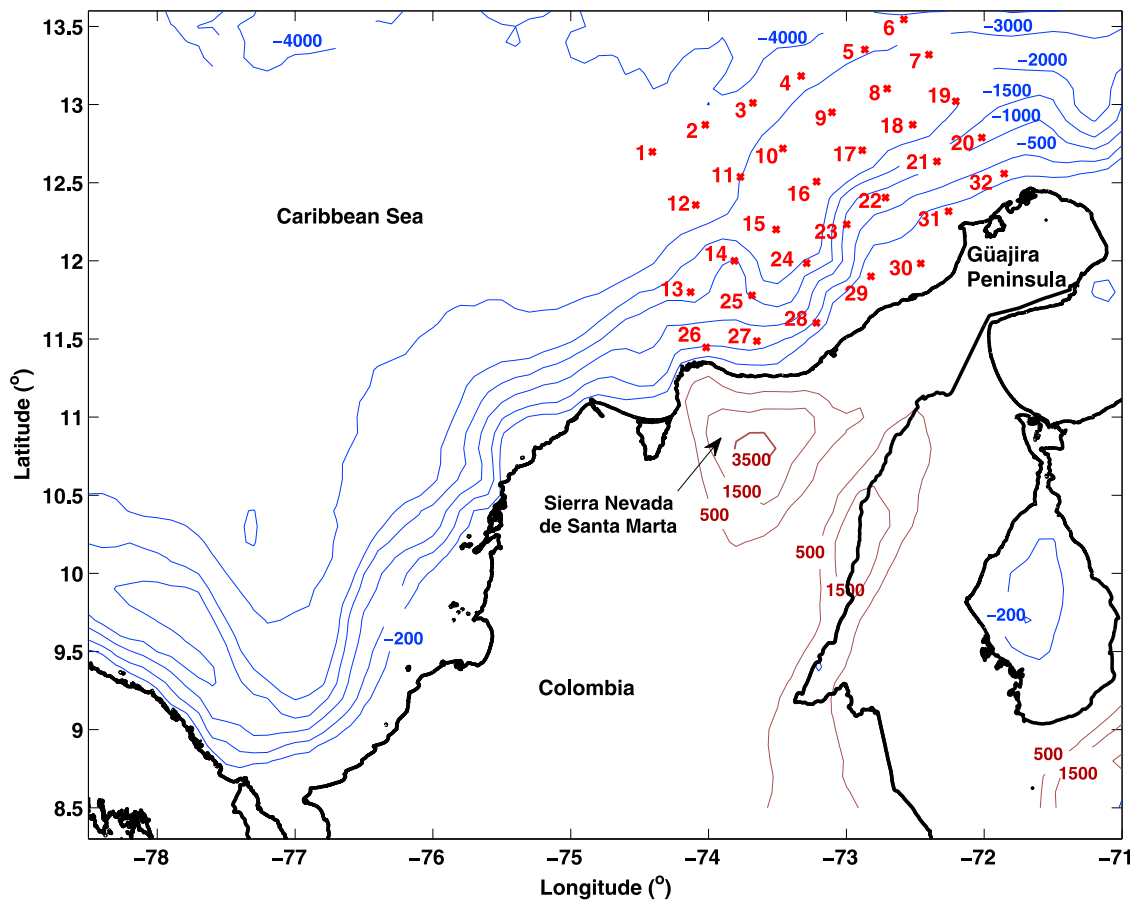


**Figure 2.** Study region: part of the Colombian Basin showing bathymetry (m), topography (m), and location of oceanographic stations.

gráficas (CIOH) in Colombia. Oceanographic stations covered an area of about  $210 \times 260$  km in the cross-shore and alongshore directions, respectively, off the Guajira Peninsula, where upwelling occurs throughout the year. A conductivity-temperature-depth (CTD) Sea Bird SBE 19 profiler was used from the surface to 300 m, sampling 8 times/s (1 m vertical resolution) as it was lowered in the water column, providing a detailed view of the vertical structure. Data quality control included manufacturer calibration of the CTD prior to the cruise and comparison with an oceanographic control station. This control station was surveyed with independent instruments (reversing thermometers and salinometers).

[9] The ocean model component was based on the curvilinear orthogonal horizontal grid and vertical sigma coordinate Princeton Ocean Model described by *Blumberg and Mellor* [1987]. The modeling system employed in the present work, developed at CIOH, consisted of a three-dimensional oceanic circulation model including 18 sigma levels with satellite data assimilation (using a Cressman successive corrections scheme) of sea surface temperature from National Oceanic and Atmospheric Administration (NOAA) satellites. The system operationally receives meteorological data from the United Kingdom Meteorological Office global high-resolution atmospheric model. Coupled with a Lagrangian transport block, the model was designed to forecast oil spills and to assist in search and

rescue efforts [*Lonin et al.*, 2003]. The spatial resolution varies between 5 and 15 km, giving best resolution over the Colombian shelf. The National Geophysical Data Center ETOPO-5 gridded topography data provided the bathymetry field in the ocean model. The modeling system was initialized with climatological temperature and salinity data from the World Ocean Atlas 2001 [*Conkright et al.*, 2002], providing a  $1^\circ$  horizontal resolution at 33 standard depth levels. In addition, climatologies from the Comprehensive Ocean Atmosphere Data Set [*da Silva et al.*, 1994] supplied the heat and stress surface fluxes for cold-start initialization.

[10] Atmospheric simulations to scrutinize the evolution of the pressure system departures were obtained from the fifth-generation Pennsylvania State University-National Center for Atmospheric Research Mesoscale Model (MM5) described by *Dudhia* [1993]. The MM5 mesoscale modeling system version 3.7 was set up for the atmosphere in two nested domains at 10 and 30 km spatial resolutions, covering a large region bounded by  $5^\circ\text{N}$ – $34^\circ\text{N}$  and  $95^\circ\text{W}$ – $70^\circ\text{W}$ , including the Colombian Basin. We took the NCEP/NCAR reanalysis [*Kalnay et al.*, 1996] of March 2003 as lateral boundary conditions in the atmospheric simulations.

[11] Since we focused on the influence of large-scale atmospheric systems in the Caribbean Basin, we consider a larger domain in our discussion. This larger domain is sufficient to explore changes in the high- and low-pressure systems in southern North America, the lower mid-Atlantic,

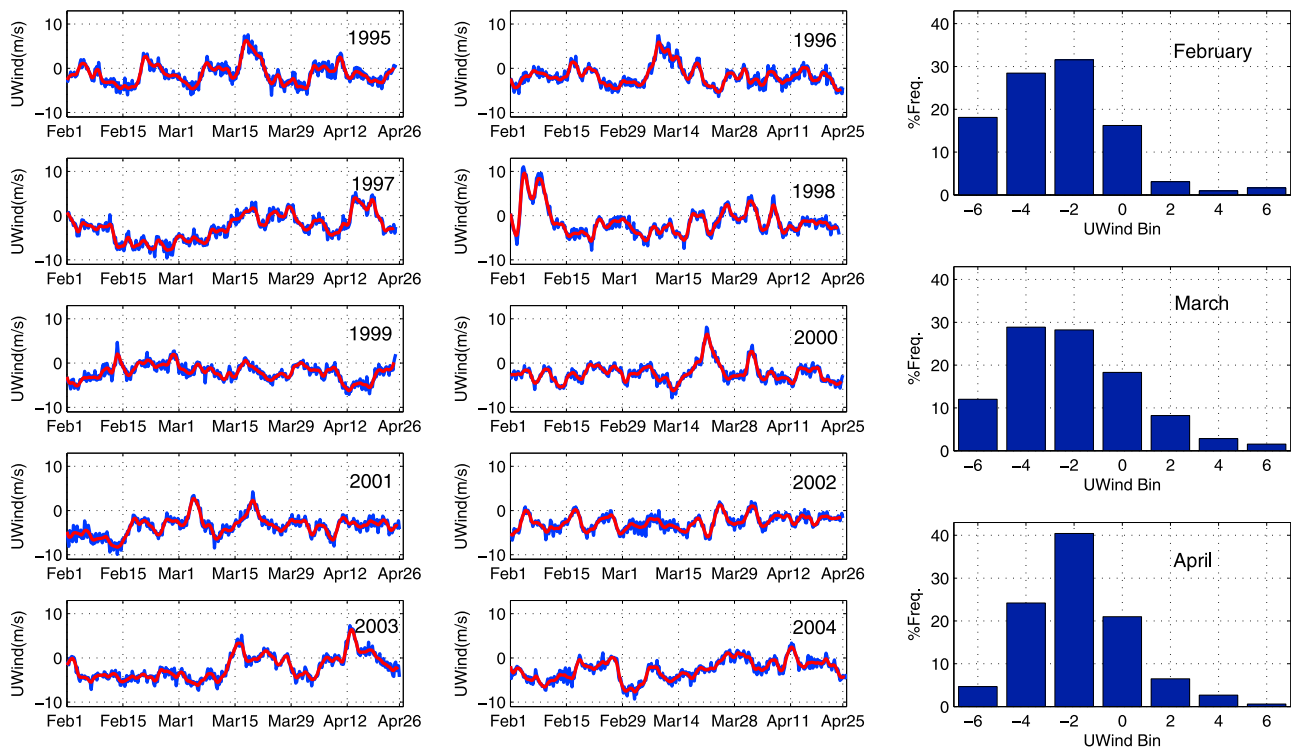


**Figure 3.** 1995–2004 NCEP reanalysis U-Wind average ( $12.5^{\circ}\text{N}$ – $15^{\circ}\text{N}$ ,  $77.5^{\circ}\text{W}$ – $70^{\circ}\text{W}$ ) during 1 February to 30 April periods. Since wind flows parallel to the Colombian coast, the U-Wind component is mainly negative in winter when stronger upwelling is expected. In March, during the winter–spring transition, the U-Wind component more frequently becomes positive. Notice examples of such strong departures in 1995, 1996, 2000, 2001, and 2003. Blue line corresponds to the daily observations, and red line corresponds to the three-point running average.

and the Caribbean. The MM5 physics considered in this investigation included the moisture scheme by *Dudhia* [1989]; the Arakawa-Schubert cumulus parameterization by *Grell and Devenyi* [2002]; and the five-layer soil temperature model, the cloud radiation scheme for atmospheric radiative transfer, and the planetary boundary layer parameterization by *Hong and Pan* [1996]. This physics configuration allows for a reasonable description of the tropical climate variability in neighboring Central America and the western Caribbean coast [*Hernández et al.*, 2006].

[12] One decade of the NCEP/NCAR reanalysis is used to study the frequency of anomalous winds in daily data in the February–April period for the years 1995–2004. We focused our attention on March, when the transition between boreal winter and spring takes place and when the observations and ocean simulations were performed.

#### 4. Results and Discussion

[13] The NCEP reanalysis data confirmed the occurrence of anomalous wind situations during the winter-to-spring transition in the southwestern Caribbean ( $77.5^{\circ}\text{W}$ – $70^{\circ}\text{W}$ ,  $12.5^{\circ}\text{N}$ – $17.5^{\circ}\text{N}$ ), as shown in Figure 3.

[14] The zonal wind component (U-Wind in Figure 3), usually negative under typical trade winds, becomes positive over periods of a few days during February–April in the 1995–2004 decade. These anomalous wind situations, when U-Wind is  $\geq 2$  m/s, are 10.8% (more frequent) in March,

8.1% in April, and 5.4% in February. In supporting our discussion of the observed changes in Guajira coastal upwelling, we first conduct an assessment of the performance of the ocean model and then present the results of the ocean model simulations. Similarly for the atmospheric model, we first conduct an assessment of the performance of the model and then present the results of the MM5 simulations.

##### 4.1. Ocean Model Evaluation

[15] The data assimilation system provided a realistic spatial and temporal representation of the oceanographic features in the Caribbean Basin and tracked the evolution of the upwelling pattern as it developed during 4 March to 9 April 2003. The Caribe 2003 cruise data, which were not assimilated into our simulations, were used for formal assessment of model performance. Since these observations were taken over a shorter period (26–30 March 2003), we were unable to assess the performance of the model simulations in the temporal dimension. Instead, we focus our evaluation on the skill in the horizontal and vertical distribution of the correlation coefficient (CC), the root mean square error (RMSE), and the bias in the Guajira coastal upwelling area.

[16] For each cruise station, we chose the closest model node to obtain simulated profiles for comparison with the corresponding observations. Preprocessing of the observational data for our analysis included performing an initial

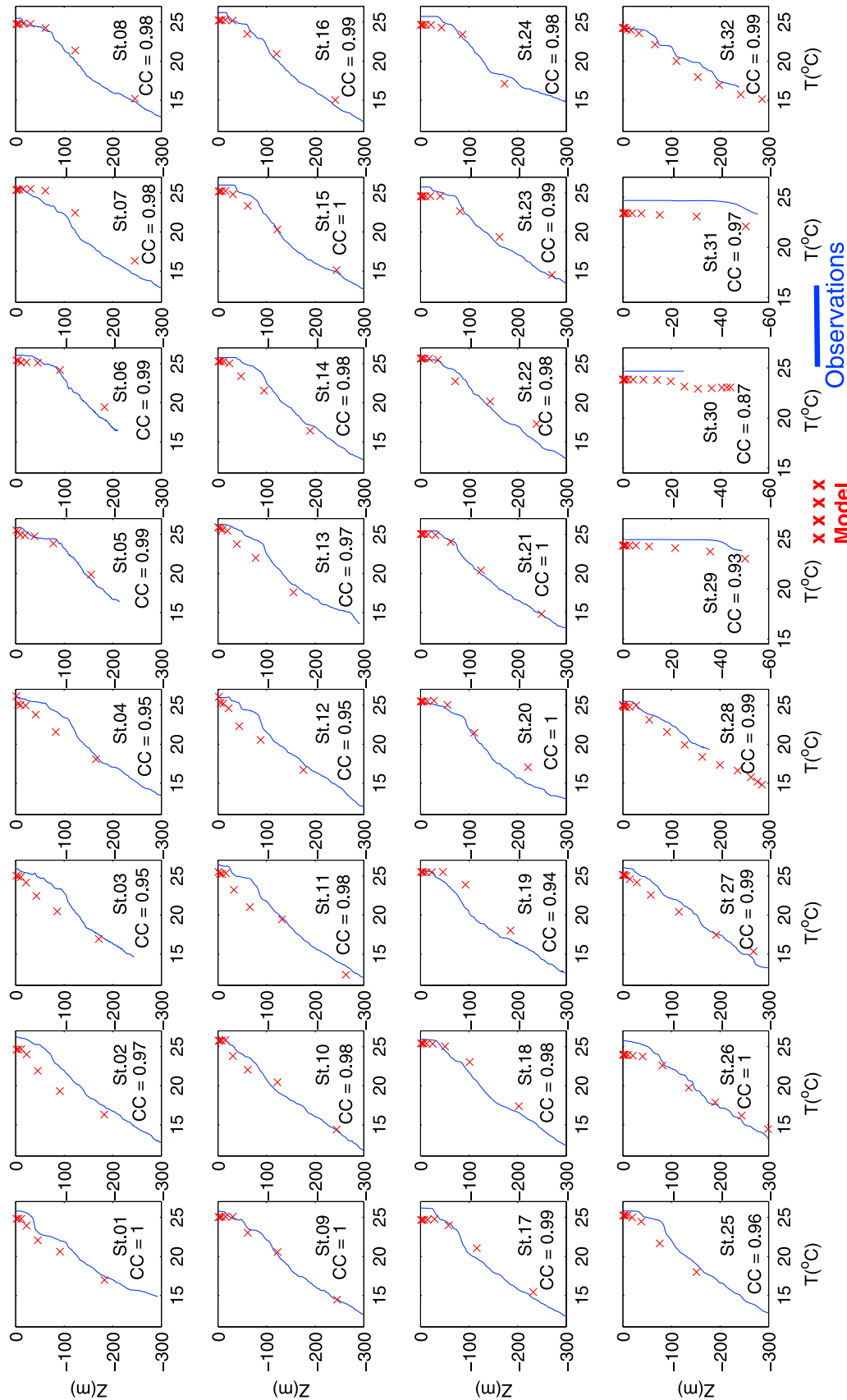


**Figure 4.** Profiles of temperature ( $^{\circ}\text{C}$ ): comparison between model and observations and CC at each station. All stations have the same vertical and horizontal axis except stations 29, 30, and 31 with depth ( $Z$ ) of  $< 100$  m.

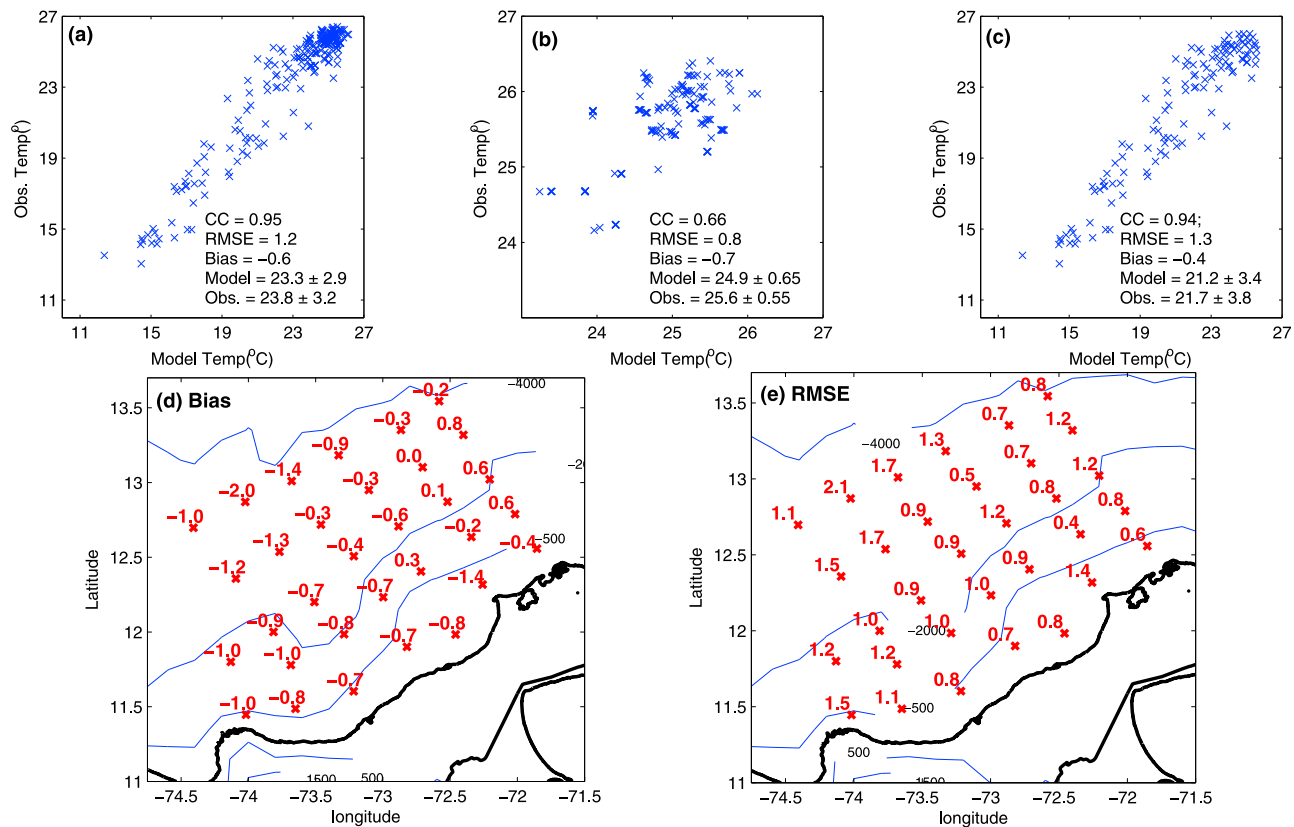


**Figure 5.** The ocean model skill for temperature is evaluated by computing CC, RMSE, bias, mean, and standard deviation applied on model and observational data. (a) The scatterplot shows all oceanographic stations in this study and presents two clusters, one with higher temperatures (mostly surface data) and a well-correlated region below the surface. (b) Surface data: upper 20 m. (c) Data below 20 m to about 300 m. (d) Bias and (e) RMSE at each oceanographic station (red cross) over-imposed on a map of ocean bathymetry.

five-point moving average for downcasts and upcasts and then applying a cubic spline interpolation to obtain measurement profiles. Figures 4 and 6 present the complete processed profiles for temperature and salinity, as well as the corresponding model profiles. Figure 4 shows a comparison of model and observed temperature profiles at the 32 oceanographic stations in this survey. All stations have the same vertical and horizontal axes, except stations 29, 30, and 31, which correspond to the shallowest stations (<100 m). Visual inspection of Figure 4 indicates that the modeling system performed adequately in describing surface and vertical temperature distributions, both in shallow coastal waters and in oceanic locations. At selected depth intervals of interest, skill analysis included computing of the CC, the RMSE, the bias, and the mean and standard deviations, as shown in Figures 5 and 7. The CC confirms a good correspondence at all stations, ranging from 0.87 to 1 for simulated temperature.

[17] Figures 5a–5e are intended to evaluate the model outputs in general (horizontally and vertically) and for particular vertical ranges. Figure 5 displays spatial model performance in terms of CC, RMSE, bias ( $\langle \text{model} \rangle - \langle \text{obs} \rangle$ ), where  $\langle \rangle$  is the average over the depth being assessed), model average and standard deviation (model), and observed average and standard deviation (obs). Figure 5a displays all

temperature station data to explore areas of distinctive correlations. There are two main clusters in the data in Figure 5a: the first cluster includes higher temperatures, mostly surface data in the upper 20 m layer (shown in Figure 5b), and the second cluster, with reasonably good correlation, is below the surface layer (shown in Figure 5c). The geographical distribution of model skill in Figures 5d and 5e presents the bias and the RMSE, respectively, at each station.

[18] According to Figures 5a–5c, the model performs well in describing surface and vertical temperature distributions. The correlation and accuracy are good for all data (Figure 5a; CC = 0.95, RMSE = 1.2) and below surface (Figure 5c; CC = 0.94, RMSE = 1.3). A lower linear association (CC = 0.66) exists at the surface, as shown in Figure 5b, with RMSE = 0.8. Model accuracy is reasonably acceptable, considering that the normalized RMSE to the observed mean ranges between 3.3% and 6.1%. In general, all vertical ranges present good agreement in terms of mean and standard deviation. According to Figure 5a, surface water temperature is typically about 25°C in the period of investigation. According to the bias in Figures 5a, 5b, and 5c, the model underestimates the observations by about 0.6°C in the vertical distributions. The spatial distribution of bias at each station (Figure 5d) ranges from -2°C to 0.8°C, revealing a tendency to be positive (0.1–0.6°C) in the

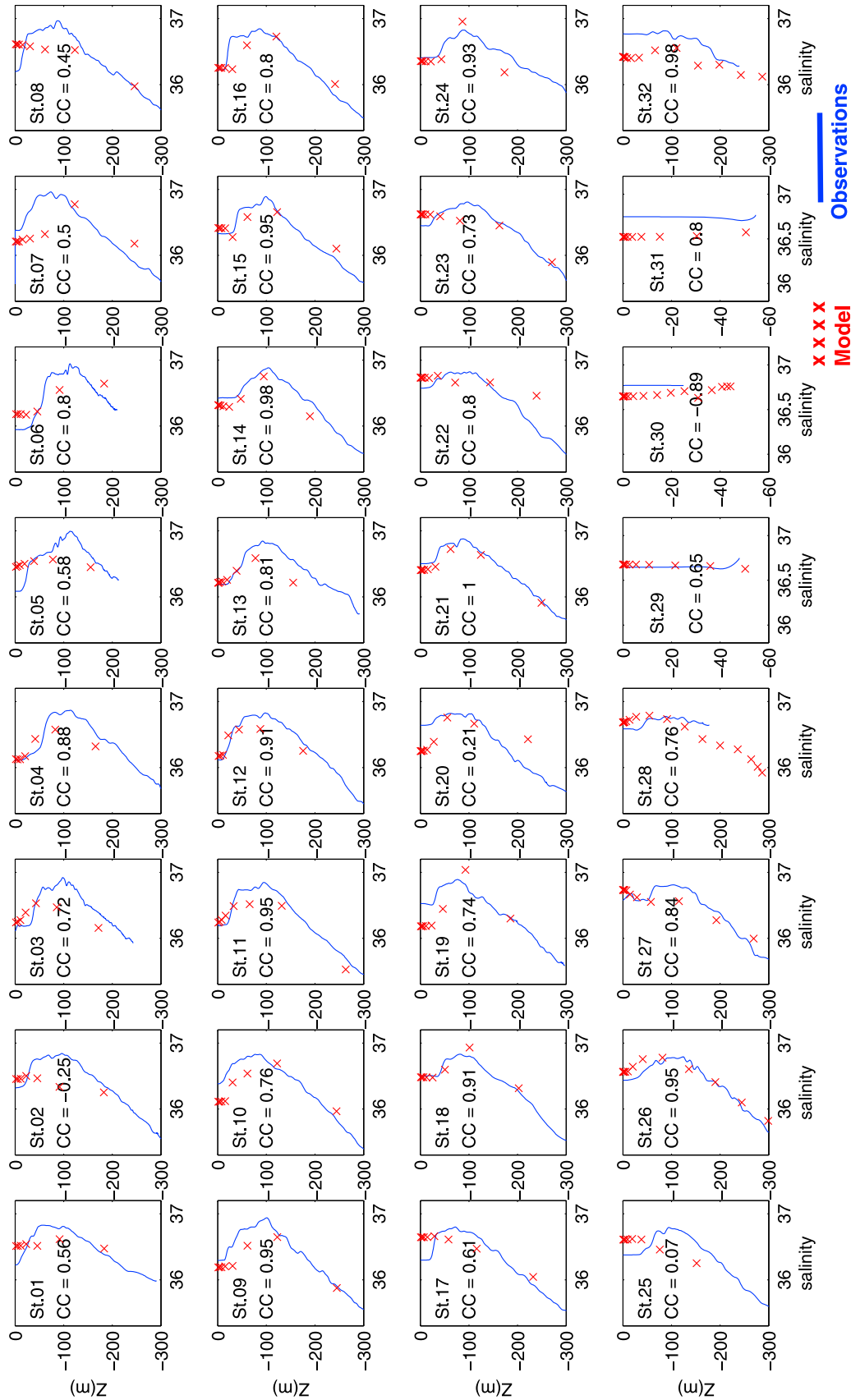


**Figure 6.** Profiles of salinity: comparisons of modeled and observed data and CC at each station. All stations have the same vertical and horizontal axis except stations 29, 30, and 31 with depth ( $Z$ ) of <100 m.

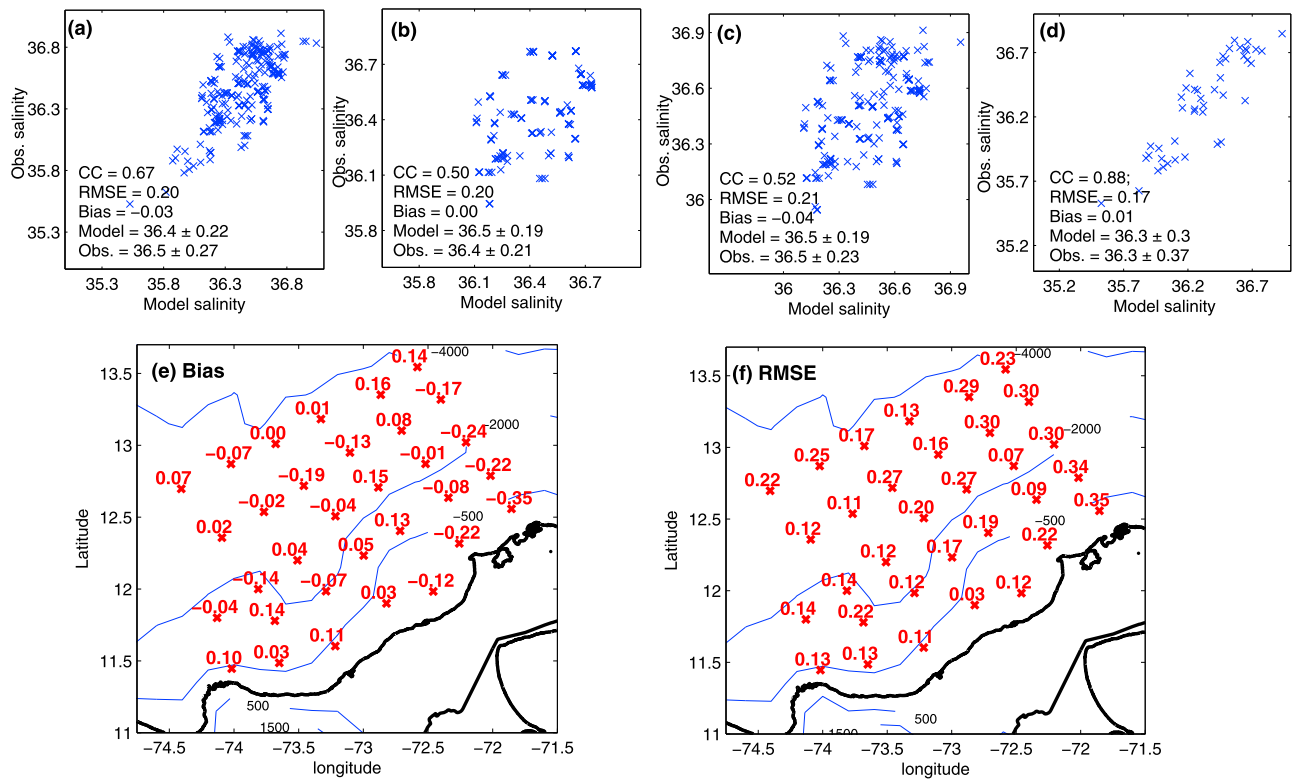


**Figure 7.** Similar to Figure 5, the ocean model skill for salinity is evaluated by computing CC, RMSE, bias, mean, and standard deviation. All pairs of observed and model data are presented in Figure 7a. We explore three regions: (b) upper 20 m, (c) upper 100 m or above salinity maximum, and (d) below 100 m depth. The geographical distributions of (e) bias and (f) RMSE at each oceanographic station.

central eastern oceanic area and negative (about  $-1^{\circ}\text{C}$ ) in most of the area. RMSE (Figure 5e) ranges from  $0.6^{\circ}\text{C}$  to  $2.1^{\circ}\text{C}$ ; however, there is not a clear pattern in the spatial distribution.

[19] There are several possible sources of error that can cause differences between the model and the observations. Biases are likely attributable to the following reasons: (1) the temperature was assimilated only at the sea surface; (2) the vertical resolution varied by location, since it was defined by a sigma level configuration; and (3) satellite data can be affected by aerosol contamination, making surface temperature lower than observed [Lonin *et al.*, 2003]. Clouds are also likely to affect model results in the Caribbean region [Anduckia and Lonin, 2004]. Cloud and water vapor effects are more noticeable in coastal areas in the Colombian Basin, where high elevations such as the Sierra Nevada de Santa Marta obstruct the trade winds and contribute to topographic cloud formation.

[20] Modeled and observed salinity profiles at the 32 stations and the corresponding CCs are shown in Figure 6. Although salinity was not assimilated but nudged to a low-resolution climatology, the modeling system qualitatively describes well the observed vertical distributions in most of the stations. There is a reasonable correlation of 0.7 or higher in 23 of the oceanographic stations, and such correlation is generally observed in areas at  $\geq 500$  m deep. Some oceanic (1, 2, 7, 8, 20, and 25) and coastal (29) stations present low CCs, likely arising from nudging to climatological salinity. Dur-

ing the Caribe 2003 cruise, salinity had an observed maximum at around 100 m and the model reasonably describes this feature at these stations. The model has terrain-following vertical coordinates that influence the vertical resolution depending on the depth. It is noticeable that in some shallow water stations (21–24, 26–28, and 30–32), with closer vertical sampling, the model yields a better representation of salinity profiles.

[21] The model skill discussion for salinity is based on the results presented in Figure 7. Figure 7 shows a statistical analysis similar to that conducted for temperature. The scatterplot in Figure 7a displays all modeled and observational data pairs to define areas of distinctive correlation. From Figure 6, it is clear that there was low salinity at the surface and a maximum of about 36.5 around 100 m in oceanic waters. This subsurface salinity maximum corresponds to subtropical underwater (100–200 m), which is exchanged through the northeast passages in the Caribbean [Wüst, 1964; Gordon, 1967]. On the basis of Figures 6 and 7a, we identified areas of interest for more detailed investigation. We used depth to define areas of higher correlations. Figure 7b shows records in the surface layer confined to the upper 20 m. Figure 7c considers data in the upper 100 m, and Figure 7d contains data below 100 m. Figure 7a displays close averages and standard deviations ( $36.4 \pm 0.22$ ,  $36.5 \pm 0.27$ ) for model and observation data, with a modest correlation of  $\text{CC} = 0.67$ . In the upper 0–20 m and 0–100 m layers (Figures 7b and 7c), the statistical outputs show

similar RMSE, bias, average, and standard deviation. However, CC is only 0.5, which is significantly lower than in Figure 7a. An improved skill pattern is obtained below 100 m, where model mean and standard deviation are close to observations ( $36.3 \pm 0.3$  and  $36.3 \pm 0.3$ , respectively), with a good correlation (CC = 0.88), a slightly positive bias of 0.01, and a lower RMSE of 0.17 relative to Figures 7a–7c. It is clear that the climatological salinity used to nudge the modeling system performs reasonably well to describe profiles below 100 m. Panels 7e and 7f help describe the geographical distribution of bias and model accuracy. There are positive and negative low biases present in the area; however, higher negative biases are present in the east, close to the peninsula. RMSE spatial distribution spans from 0.03 to 0.35, following a similar pattern to that of the bias, with a lower accuracy close to the peninsula. Therefore, actual data would be needed in the upper 100 m to improve the model performance in future efforts.

[22] To analyze the effect of the possible sources of error (low vertical resolution in salinity and the influence of aerosols in satellite-derived temperature), we consider the characteristic times for the vertical turbulent diffusion and the vertical advection (convection or upwelling) in the upper ocean layer. Typical wind speeds of  $\sim 10$  m/s generate mixed layer depths ( $h$ ) ranging from 10 to 50 m. These values yield a friction velocity ( $u_*$ ) of  $0.5 \times 10^{-2}$  m/s and a turbulent diffusion ( $K_z = \kappa u_* h$ ;  $\kappa \approx 0.4$ ) ranging from 60 to 300  $\text{cm}^2/\text{s}$ . Under such conditions, the characteristic time of turbulent diffusion ( $T_{\text{diff}} = h^2/K_z$ ) is 0.5–2.3 h. On the other hand, the typical model vertical velocities ( $w$ ) of  $10^{-3}$  m/s in the upwelling zone yield a characteristic vertical advection time ( $T_{\text{adv}} = h/w$ ) of 2.7–14 h. It is clear that the time scale of  $T_{\text{adv}}$  (upwelling) is an order of magnitude higher than  $T_{\text{diff}}$  (vertical turbulent diffusion), which explains why temperatures along vertical profiles are somewhat underestimated.

[23] Although clouds are a main source of aerosols, the Guajira Peninsula and most of the extreme northern part of South America present an arid regime, such that local marine and mineral dust aerosols can also potentially affect quality in satellite-derived surface temperatures. In this regard, Kaufman *et al.* [2005] present MODIS Terra aerosol optical depth observations in March 2003 (and other years as well), confirming higher columns of dust and smoke around the Colombian land and ocean. Another important point, recently brought up by Liu *et al.* [2008], is that wind power density presents a remarkable peak at the Guajira Peninsula. Because of this, aerosol transport into the western Caribbean from the peninsula can be more significant than global aerosol transport models typically predict. A high-resolution modeling approach recognizing regional land surface and soil characteristics could provide better estimates of aerosol emissions and transport to evaluate concomitant contamination in sea surface temperature measured from satellites and data assimilation experiments involving remote sensing data. In fact, this becomes an interesting field of investigation to enhance predictability of weather and climate variability in the Caribbean region. Finally, the most important source of dust for the Caribbean, the Sahara desert, does not coincide in time and location with the studied event and has its major impact at higher latitudes (about 18°N), with an annual peak in June [see Prospero *et al.*, 2002].

## 4.2. Response to the Atmospheric Disturbance in the Ocean Model

[24] Figure 8 shows a sequence of model surface distributions for sea surface temperature (first column), surface salinity (second column), sea level (third column), and vertical velocity at 50 m (fourth column). These 2-day average distributions present the evolution of the surface oceanographic conditions starting with moderate upwelling (5–6 March, first row), strong upwelling (12–13 March, second row), disrupted upwelling during the atmospheric event of 18–19 March (third row), and restored conditions (1–2 April, fourth row). The first, second, and fourth rows in Figure 8 clearly display the typical distribution of coastal upwelling at the Guajira Peninsula with lower temperatures, higher salinities, and positive (upward) vertical velocities, respectively.

[25] Upwelling was most developed on 12–13 March, when a large patch of cold, salty waters covered most of the northern Colombian coast. As has been found in previous investigations [e.g., Mooers and Maul, 1998; Andrade *et al.*, 2003], the upwelling process is limited to 14°N in the north because of the effect of the westward Caribbean Current and to 11°N in the south because of the effect of the Panama-Colombia cyclonic gyre, which occupies the southwestern portion of the Colombian Basin. According to the present simulation, the Panama-Colombia gyre brought warmer, less saline waters into the region. These less saline waters are mainly the product of higher annual precipitation in the west and southwest areas of the Caribbean, as shown by some of the earliest investigation in the region [e.g., Wüst, 1964]. While it is well known that evaporation and precipitation are additional factors that affect surface salinities, modeling precipitation and its impact on regional sea surface is outside the scope of the present work. Our oceanographic and atmospheric models were run separately, and thus, the current data assimilation system cannot explain the effect of precipitation on ocean surface salinity; subsequent investigations should implement a modeling system consisting of coupled ocean and atmosphere components.

[26] During 12–13 March, the cyclonic gyre was located to the southwest of the study region, but on 18–19 March, it extended northward, pushing the upwelled waters against the coast and restricting them to the northernmost part of the Guajira Peninsula. Sea surface level in the upwelling zone is more negative than in the rest of the region, as expected. When the atmospheric disturbance occurred and the coastal upwelling was pushed northward, the sea levels increased to 0 cm in areas of otherwise persistent upwelling. Sea surface levels closer to 0 cm are concurrent with low wind stress transmitted to the ocean surface, as shown in Figure 9. Vertical velocity is expected to be positive in upwelling areas. Under normal upwelling conditions, positive values are more spread out over the region as manifested on 5–6 March, 12–13 March, and 1–2 April, with a persistent peak at the northernmost tip of the peninsula. Negative values are characteristic at the southwest, coinciding with the Panama-Colombia gyre. A more fragmented vertical velocity distribution is evident on 18–19 March, when patches of negative velocities expanded and extended along the coast.

[27] Surface air-sea energy exchange is presented in Figure 9, which contains a sequence of surface energy

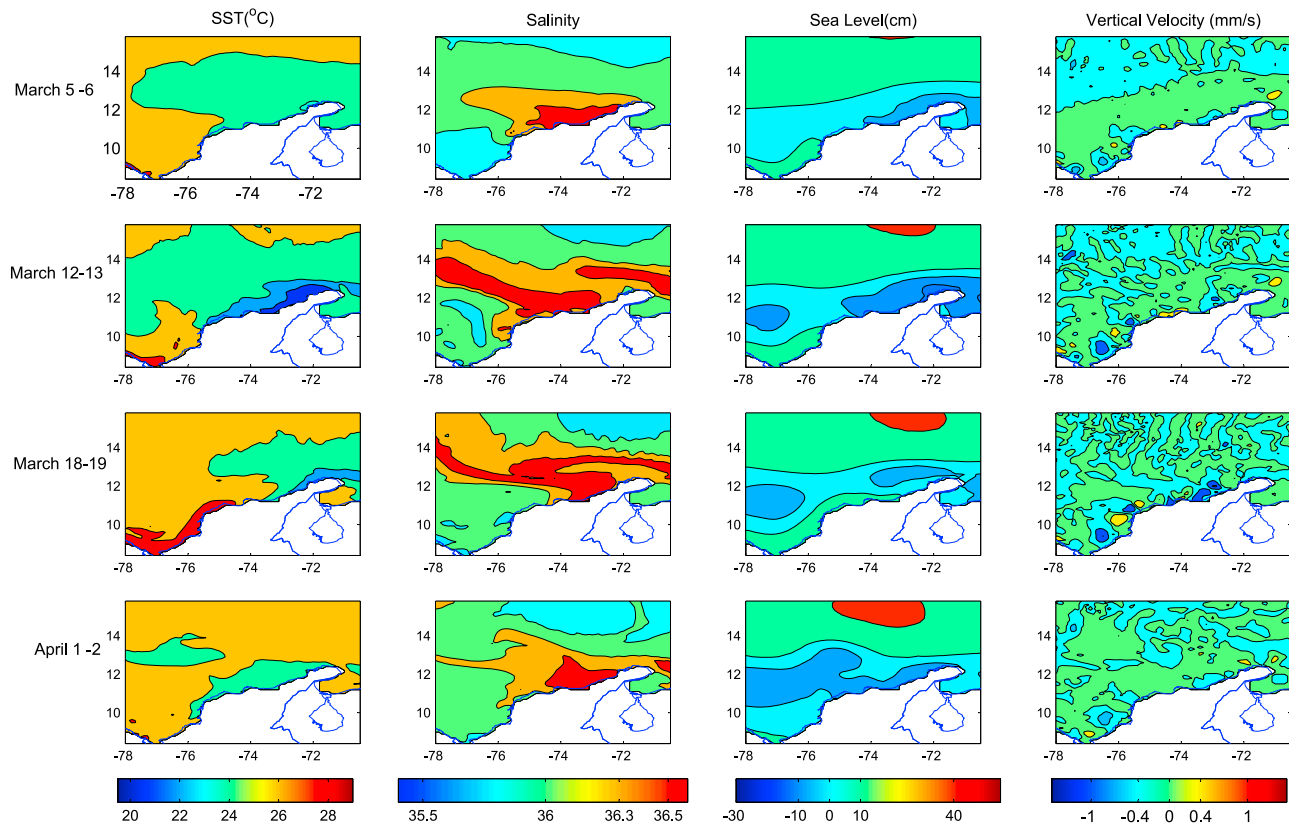


**Figure 8.** Sequence of modeling results for sea surface temperature ( $^{\circ}\text{C}$ ), salinity, sea level (contour levels in cm at  $-25$ ,  $-10$ ,  $0$ ,  $10$ , and  $40$ ) and vertical velocity ( $\text{mm/s}$ ) corresponding to 2-day averages as indicated. Model outputs clearly indicate changes in surface conditions by the time of the event (18–19 March 2003), particularly stronger in temperature and salinity distributions.

fluxes for wind stress (first column), sensible heat flux (second column), and latent heat flux (third column) in selected 2-day averages over the study period.

[28] There are noticeable changes in the energy fluxes before, during, and after the atmospheric event. The conventional and widely used method for estimating wind stress, sensible heat, and latent heat between the ocean and the atmosphere is by using bulk parameterization formulae of the near-surface layer [Cayan, 1992]. Wind stress, the primary mechanical energy source for ocean currents, is clearly stronger in the typical (first two upper panels) and restored (fourth) upwelling conditions, averaging  $0.06$ – $0.12 \text{ N/m}^2$  in most of the region with a vigorous area along the Colombian coast, where it reaches about  $0.2 \text{ N/m}^2$ . Weak wind stress dominates during the atmospheric event. Such low wind stress explains the corresponding enhanced sensible heat due to a higher sea-air temperature gradient and depleted latent heat release throughout the region. Areas where upwelling is more likely to take place (northern and central Colombian coast) show a sensible heat transfer to the ocean (negative) being particularly important during strong upwelling conditions (12–13 March), with energy fluxes between  $-30$  and  $-60 \text{ W/m}^2$ . Sensible and latent heat fluxes seen on 19 March are comparable to the other dates. There are two contrasting patterns of latent heat flux in the region under typical atmospheric conditions: one in the Guajira region with higher winds and lower humidity and another in the southwest close to Panama, where higher humidity and

lower winds are typical throughout the year. Because of that, during 5–6 March, 12–13 March, and 1–2 April, a lower latent heat is released to the atmosphere in the Guajira but higher in the southwestern area.

[29] The disrupted upwelling was driven by an atmospheric disturbance that lasted about 3 days as revealed by daily mean SLP observations from NOAA National Climatic Data Center (NCDC) Global Surface Summary of Day (GSOD; available at <ftp://ftp.ncdc.noaa.gov/pub/data/ggod>) data during March 2003. This data set contains many stations in the Caribbean region; however, several of them consist of incomplete records during the studied period. To estimate the duration of the event, we chose six meteorological stations to the north of the Colombian Basin in the area most influenced by the atmospheric disturbance and with noticeable pressure change. Time series in Figure 10a show SLP at those meteorological stations shown on a map in Figure 10b. This set of stations will be considered in the MM5 model evaluation. Figure 10 confirms that the pressure perturbation comes from a higher latitude since Miami observed a longer period ( $\sim 5$  days) with higher variability ( $1013.5 \pm 3 \text{ mb}$ ) for this event, followed by the southern stations at Kingston ( $1013 \pm 1.3 \text{ mb}$ ) and Guantanamo ( $1014.2 \pm 1.3 \text{ mb}$ ). San Andres, a small island (area =  $26 \text{ km}^2$ ), also displays a depression in SLP on 18 March and corroborates that the atypical pressure reaches the western Caribbean at lower latitudes. There is no record of SLP at San Andres on 19 March. Time series at Bar-

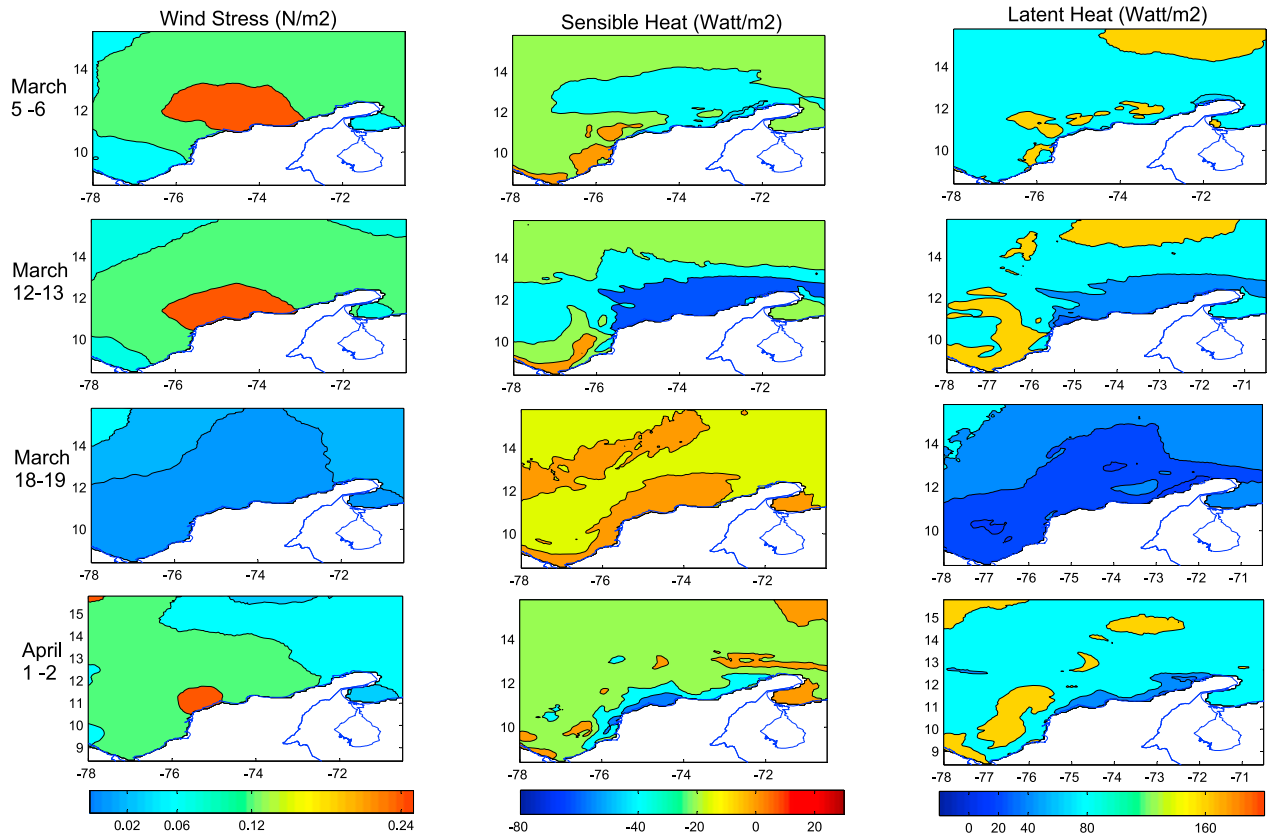


**Figure 9.** Sequence of model results for surface energy fluxes: wind stress (N/m<sup>2</sup>), sensible heat (W/m<sup>2</sup>), and latent heat (W/m<sup>2</sup>). Lowest wind stress and latent flux with positive sensible heat are manifested during the event (18–19 March 2003). Under typical condition, moderate to strong wind stress is observed in coastal areas of the Colombian Basin, except areas close to Panama.

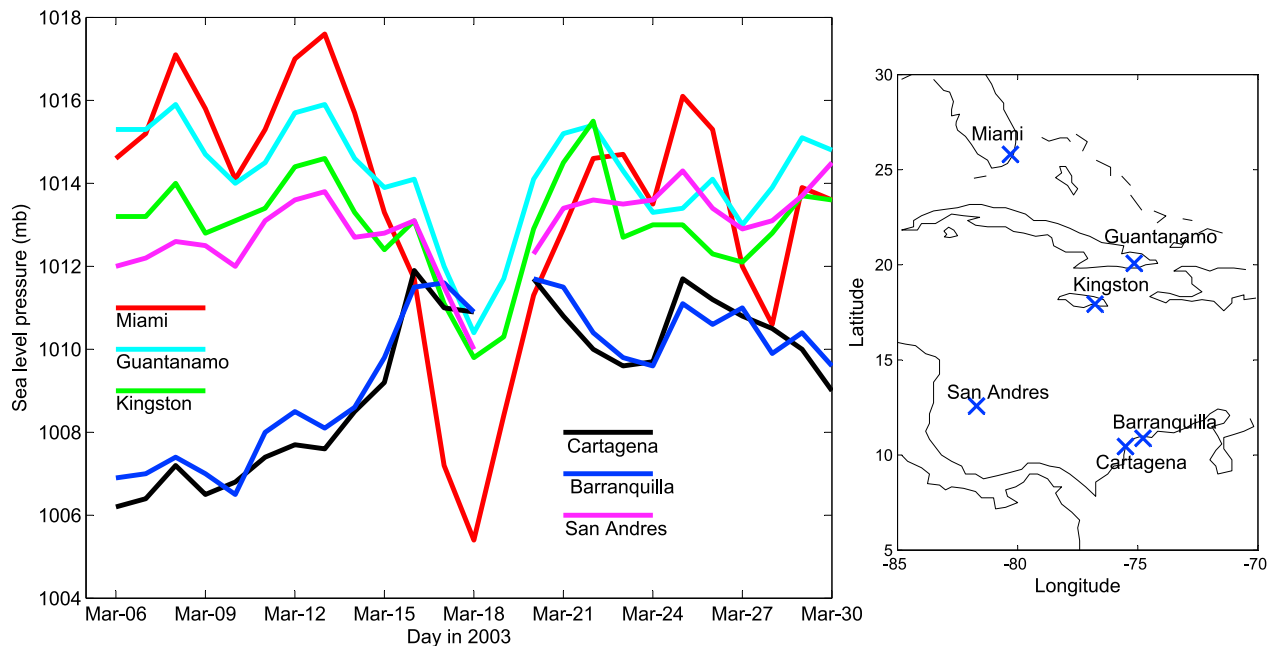


**Figure 10.** NOAA NCDC GSOD, (left) mean SLP, and (right) location of meteorological stations considered for atmospheric model skill. The depression in pressure originated at higher latitudes. The Miami station displays the highest depression of about 8 mb, compared to 3.5 mb in Guantanamo and 3 mb in Kingston, with respect to the March average conditions.

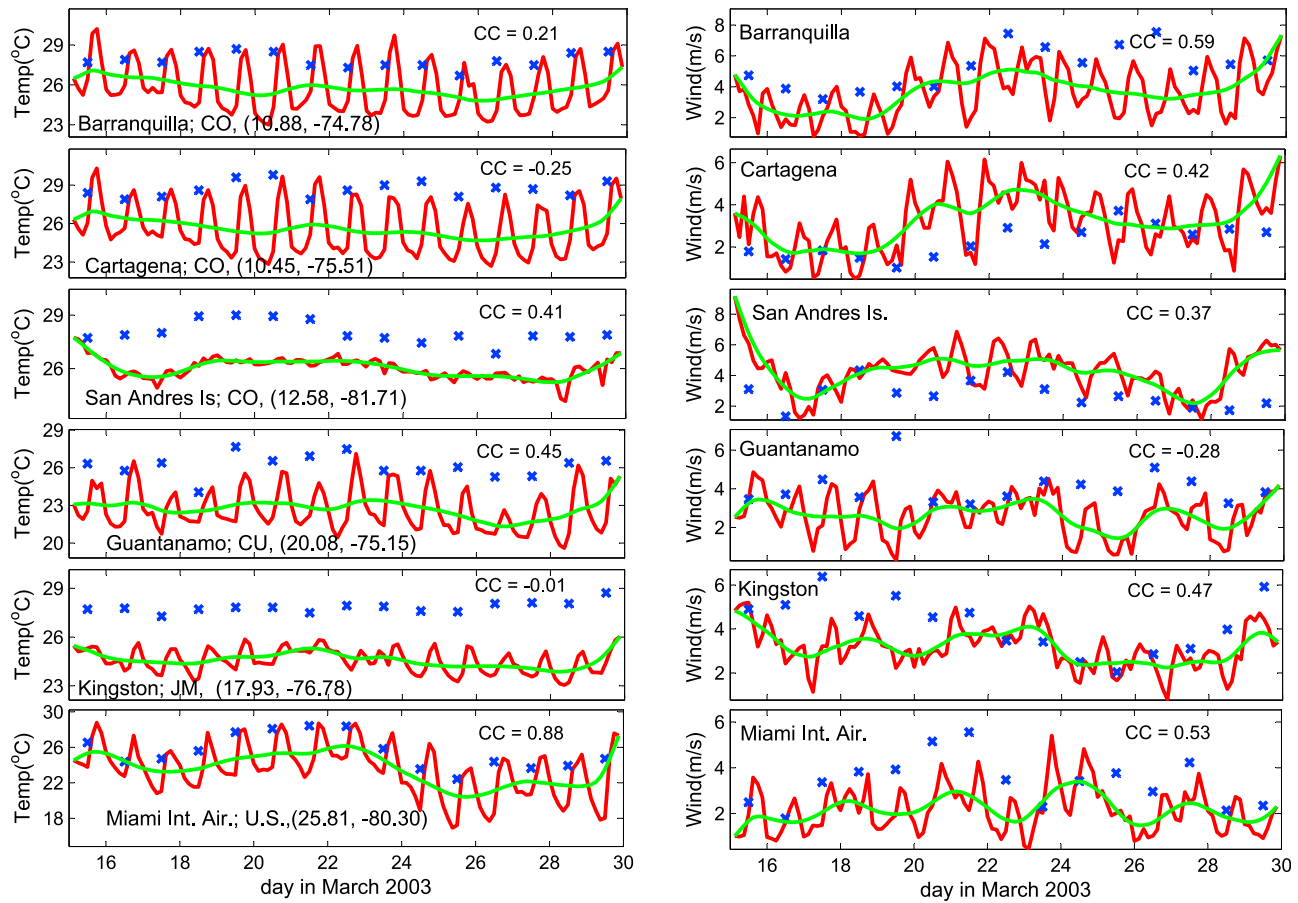


**Figure 11.** MM5 model skill assessment. Time series at six stations showing 3 h model results (red curve), eight-point moving average for MM5 results (green curve), and GSOD daily average observations (blue cross).

ranquilla and Cartagena (lowest latitude stations) present a different pattern of variability more influenced by the ITCZ and low-pressure systems in northern South America. Although there is a lack of records on 19 March at these two stations, they showed a significant increase in SLP at the time when the event occurred, attributable to a reaction to that depression at higher latitudes.

### 4.3. Mesoscale Atmospheric Model Evaluation

[30] We use the MM5 mesoscale model to explore regional atmospheric conditions. As mentioned in section 3, we used one set of physics schemes applied to both geographical domains (10 and 30 km resolutions) since we were more interested in exploring the synoptic to regional features of the pressure systems than in providing a detailed description of small-scale and local scale climate variability in our numerical experiments. We selected the physics configuration based on previous work by *Hernández et al.* [2006], which can reasonably be extended to tropical regions in America. A detailed prediction of climate parameters at subregional and local scales using a mesoscale atmospheric model would require sensitivity tests using different sets of physics schemes according to target areas, updating land use cover maps, and, for a good description of local and short-term climate variability, a data assimilation procedure [Dudhia, 1993]. A detailed representation of

small-scale (few kilometers) and short-term (less than 1-day periods) variability is beyond our goals. We present the MM5 performance assessment based on a statistical analysis for model results and the independent GSOD observational data set described at the end of section 4.2.

[31] The MM5 model performance assessment is discussed considering Figure 11 and Table 1. The MM5 results are evaluated at six meteorological stations in the region most influenced by the atmospheric perturbation studied here. According to the MM5 event evolution maps (Figure 12), that region spans about  $85^{\circ}\text{W}$ – $74^{\circ}\text{W}$ . The stations (located in the United States, Cuba, Jamaica, and Colombia), their country abbreviation, and their latitude and longitude are included in Figure 11 (right). Each panel includes the corresponding CC for each station observed and the model time series. Since all stations are located in coastal environments, they are likely expected to have a noticeable daily variability mainly controlled by sea-land breeze systems (SLBS) [Hunter et al., 2007]. The atmospheric model was set to generate 3 h results during 15–30 March 2003, and the daily cycle is clearly observed in the 2 m air temperature (right) and 10 m wind speed (left) time series. Our analysis on MM5 model accuracy at short-term variability (hours) is limited, since there is no available hourly historical data at all six stations in March 2003. Figure 11 displays an eight-point moving average of model results to facilitate com-

**Table 1.** MM5 Model Skill Assessment Using Meteorological Stations in a Region Highly Influenced by the Atmospheric Event That Perturbed the Guajira Coastal Upwelling

Station	Temperature				Wind Speed			
	Model (°C), Mean ± SD	Observed (°C), Mean ± SD	Bias	RMSE	Model (m/s), Mean ± SD	Observed (m/s), Mean ± SD	Bias	RMSE
Barranquilla, CO	25.80 ± 0.60	27.85 ± 0.56	-2.05	2.17	3.71 ± 1.09	5.27 ± 1.37	-1.55	1.90
Cartagena, CO	25.63 ± 0.65	28.69 ± 0.61	-3.05	3.20	3.25 ± 1.02	2.26 ± 0.75	0.99	1.37
San Andres Island, CO	26.03 ± 0.50	28.03 ± 0.62	-2.0	2.09	4.32 ± 1.14	2.76 ± 0.87	1.55	1.91
Guantanamo, CU	22.75 ± 0.62	26.16 ± 0.90	-3.41	3.51	2.66 ± 0.58	4.08 ± 0.91	-1.42	1.84
Kingston, JM	24.59 ± 0.42	27.84 ± 0.33	-3.25	3.29	3.18 ± 0.66	4.20 ± 1.28	-1.02	1.50
Miami International Airport, USA	23.60 ± 1.73	25.50 ± 1.94	-1.90	2.10	2.17 ± 0.51	3.38 ± 1.09	-1.21	1.50

parison with observations. Model skill performance is summarized in Table 1, including model and observational statistics (mean, standard deviation, bias, and RMSE).

[32] It is apparent from Figure 11 that Miami’s temperature and wind and Barranquilla’s winds tend to better follow daily observations, which are confirmed by the higher CC of

0.88, 0.53, and 0.59, respectively; however, that behavior is not clear in other stations and variables. In general, considering the bias columns in Table 1, the atmospheric model underestimates the observed temperature by 2.61°C on average, while wind speed is overestimated at Cartagena and San Andres (about 1.27 m/s) but underestimated at Bar-

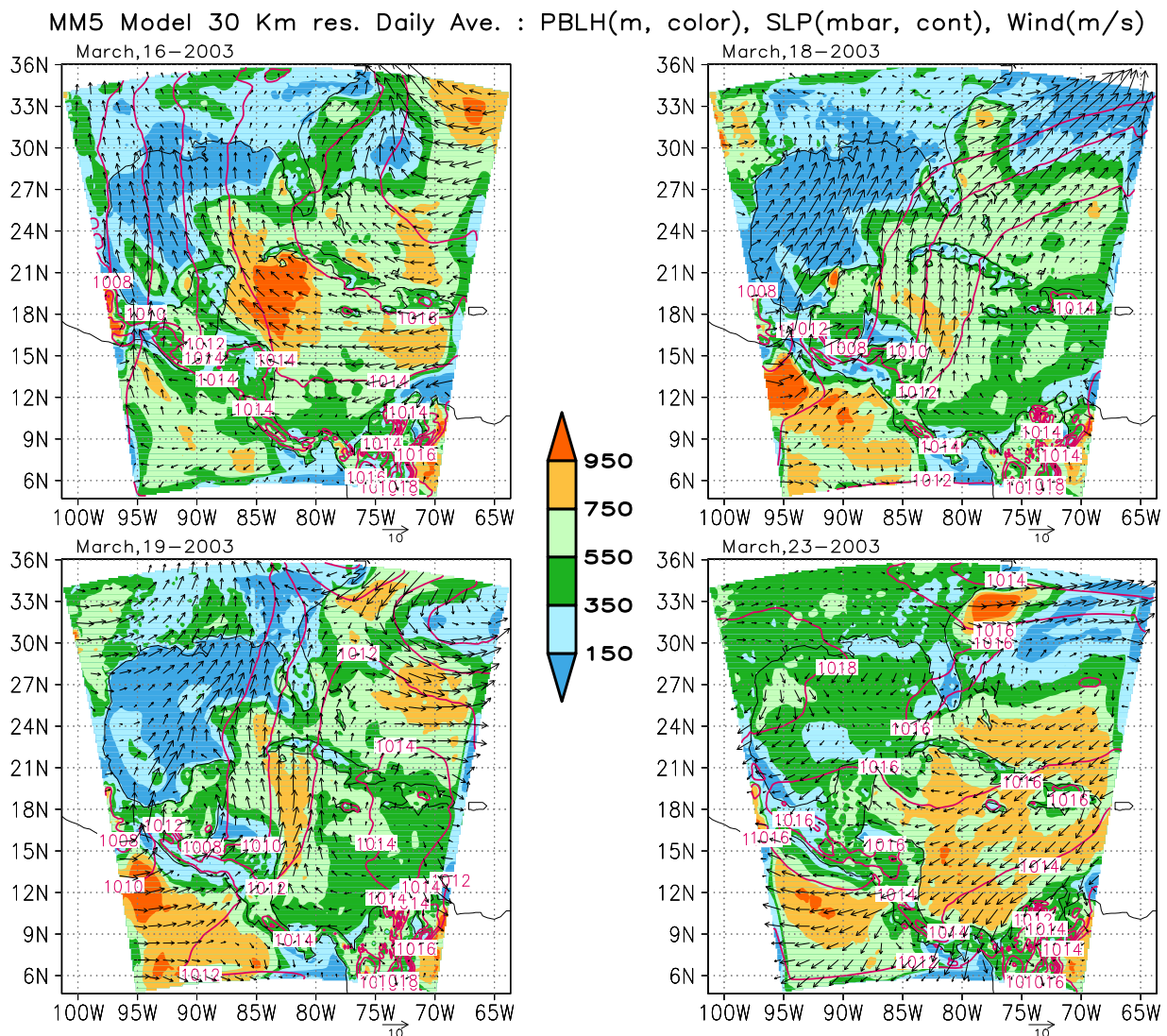


**Figure 12.** MM5 regional model results: PBLH (m, color), SLP (mb, contour), and wind vectors. Typical conditions of wind parallel to the coast (16–23 March) are disrupted by regional departures of SLP changing wind direction northward (18–19 March).

ranquilla, Guantanamo, Kingston, and Miami (about 1.3 m/s). For temperature, the percentage of RMSE ( $100 \times \text{RMSE}/\text{observed mean}$ ) has a moderate range from 8% (Miami) to 13% (Guantanamo), but it is significantly higher for wind speed from 36% (Kingston) to 69% (San Andres). According to regional modeling studies, setting such models to explore a large region like the one we are studying with nested domains would likely require changing the physics configuration and tuning the land-atmosphere exchange coefficients for a better description of environmental variables [Dudhia, 1993]. As future work, we plan to investigate MM5 model sensitivity to various physics configurations in the study region. Since SLBS are driven by differential heating between adjacent land and sea masses [Hunter, 2007], modeled temperature and wind in coastal environments are influenced by how realistic the temperature gradients are estimated from NCEP reanalysis input data. We have not explored the sensitivity of temperature and wind variability to different sea surface temperature products available for regional climate models; this is another possible source of error in the MM5 results particularly affecting the description of coastal environments.

#### 4.4. Response to the Atmospheric Disturbance in the Atmospheric Model

[33] For the MM5 simulation results, we focus our attention on two regimes in the studied period: (1) when easterly trade winds prevail in the Caribbean region, forcing the coastal upwelling, and (2) when wind direction is drastically modified, disrupting the upwelling pattern and restricting it to the northernmost part of the Guajira Peninsula. To discuss the atmospheric conditions, we consider the daily average of 10 m wind, SLP, and planetary boundary layer height (PBLH). PBLH is controlled by the vertical transport of moisture and heat, which allows the formation of clouds and eventual precipitation. Since winds are a main source of mixing, they contribute to enhance the PBLH.

[34] The evolution of atmospheric conditions over a large region including the Caribbean Sea and extending into the midlatitudes in the Atlantic is shown in Figure 12. Our discussion incorporates surface winds, SLP, and PBLH as obtained from MM5 simulation. The daily average atmospheric conditions on 23 March 2003 show stronger easterly winds prevailing in the Colombian Basin enhancing PBLH to reach 750 m. At the same time, the 1014 mb contour drives the wind direction to flow parallel to the Colombian coast promoting stronger coastal upwelling. The disruption starts around 16 March, as observed in the Miami station mean SLP time series (Figure 10), when oceanic winds between Cuba and central America bend northward, increasing their intensity and deepening PBLH. On the same day, lower wind speeds than on 23 March blow parallel to the Colombian coast, although still sustaining the Guajira upwelling system. By 18–19 March, the easterly wind pattern disappears due to a radical change in the isobars, which bend completely northward in the western Caribbean. On 19 March, the lowest PBLH is observed and weakened wind speeds are displayed over the Colombian Basin. During this 2–3 day anomalous surface pressure situation in the Colombian Basin, the winds (direction and speed) barely support the coastal upwelling, and we refer to this as a disruption to the Guajira coastal upwelling system.

[35] On 23 March, the surface wind distribution suggests the existence of a low-level jet (LLJ) in the Colombian Basin. The LLJ promotes vertical mixing in the atmosphere and in the upper layer of the ocean, significantly contributing to the mass and energy transfer between both reservoirs. Figure 13 presents the atmospheric meridional cross sections at 72°W for zonal winds (U-Wind component) and confirms the occurrence of the Caribbean LLJ. The vertical axis in Figure 13 shows the MM5 vertical sigma levels and the horizontal axis latitude. The lowest sigma level ( $\sigma=1$ ) represents an isobar at 1000 mb (about 110 m height), while the highest sigma level ( $\sigma=0$ ) corresponds to 100 mb. The presence of a westward (negative) LLJ on 16 March is clear between the surface and 0.8 sigma level (about 820 mb) and on 23 March is clear between the surface and 0.2 sigma level (280 mb). The LLJ disappears during 18–19 March, when coastal upwelling was restricted to the northernmost part of the Guajira Peninsula. Figure 9 complements our discussion for the ocean surface energy fluxes. When the LLJ disappears on 18–19 March in the atmospheric model simulation, the ocean model presents a very low wind stress, high sensible heat (energy transfer controlled by the temperature gradient), and very low latent heat transfer, causing the shallowest planetary boundary layer depth, as Figure 12 (left) indicates.

#### 5. A Conceptual Model for Event-Scale Atmospheric Disruption of Upwelling Conditions in the Southwestern Caribbean

[36] According to the NCEP reanalysis and GSOD data, the sporadic events that interrupt the normal upwelling pattern last about 2–3 days and tend to occur during the transition between boreal winter and spring. During this period, a synoptic system with two independent high-pressure centers, one over the mid northern Atlantic and the other one over the American continent, and a low-pressure center over the eastern United States and Canada may show abrupt changes at scales of days that allow surface transport of tropical warmer air toward North America crossing the Gulf of Mexico. Such events coincide with a disappearance of the high-pressure system over central North America, accompanied by low pressure moving southward in the western mid-Atlantic.

[37] The basic concept for these disruptive events has the following sequence. During boreal winter, the ITCZ is far into the Southern Hemisphere. The nearest frontal system to the north, the Subtropical Planetary Frontal Zone (SPFZ), is relatively close to the region (29.7°N on average) but is blocked by the Azores High, and therefore, the atmospheric perturbations documented in this study are not possible. In contrast, during summer, the SPFZ moves northward to about 40°N–50°N (41.3°N on average), while the ITCZ is located over the western Caribbean, so that southerly winds govern over the Mosquitos and Darien basins inside the equatorial air mass. Thus, the Panama-Colombia gyre is intensified, while the Guajira upwelling is weakened. However, since the influence of the ITCZ does not extend over the entire western Caribbean (because its effects are weaker over the water than over the continent because of the distinct stratification of the near-surface layer), the Guajira upwelling is weaker in comparison with the winter season,

MM5 Model 30 Km res. Daily Ave. : 72W Cross Section U-Wind (m/s)

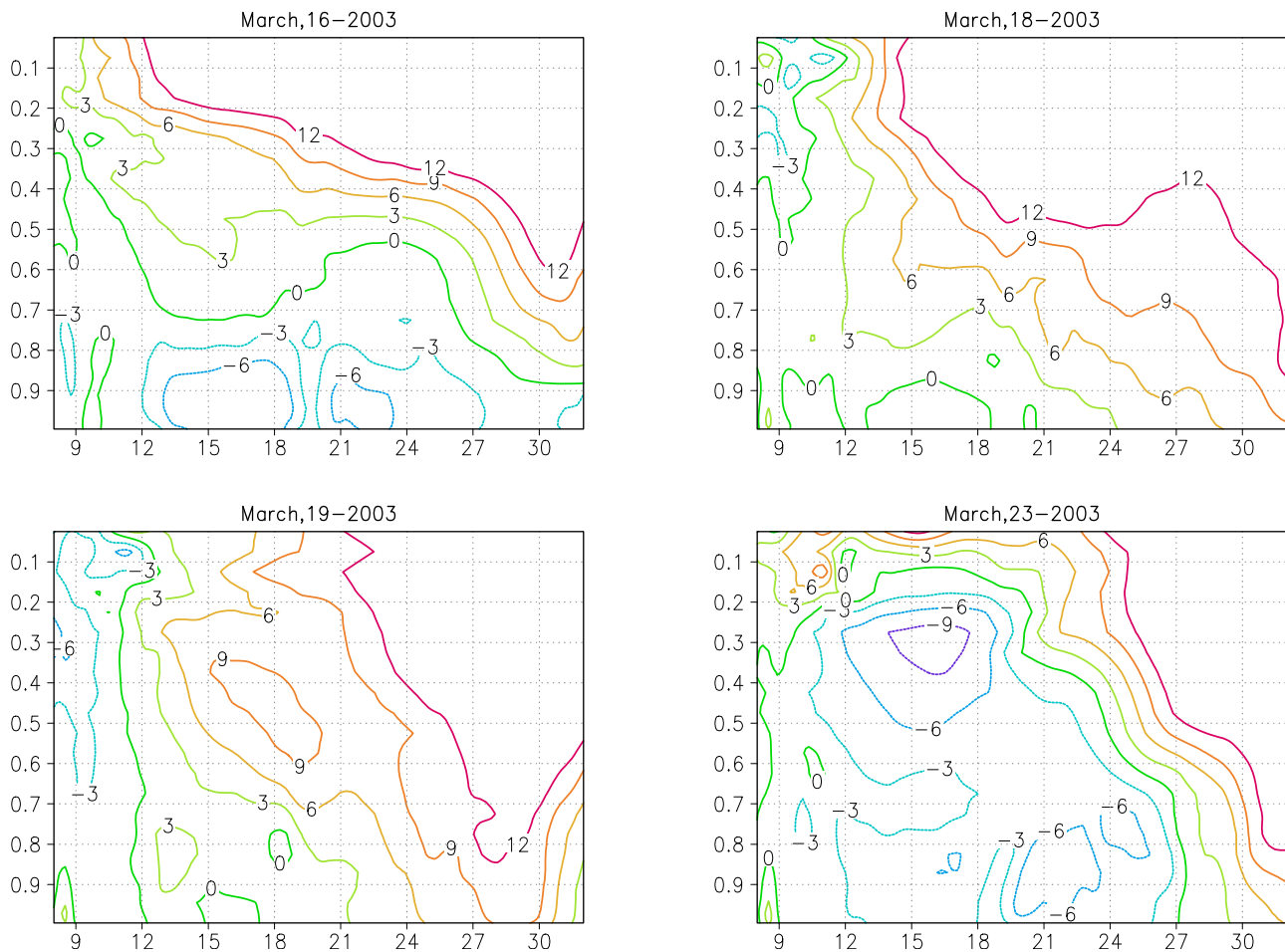


**Figure 13.** Zonal wind component (U-Wind) from the MM5 regional model at 30 km spatial resolution. Cross-meridional sections at 72°W. The vertical axis corresponds to the sigma pressure levels, and the horizontal axis corresponds to latitude. Notice the LLJ flowing westward under typical atmospheric conditions on 16 and 23 March 2003.

defining in this way the annual cycle of upwelling intensity. Disrupted upwelling is only possible during the transitional periods of the year (autumn and spring), when a confluence between the ITCZ and SPFZ can occur.

## 6. Conclusion

[38] This work has discussed ocean and atmospheric modeling experiments, their evaluations, and an atmosphere-ocean event that disrupted the normal year-round upwelling pattern off the Guajira Peninsula during the boreal winter-to-spring transition. The data assimilation modeling system has an acceptable description of the temporal and spatial evolution of oceanographic features in the region, including the three-dimensional description of coastal upwelling. The mesoscale model explained the atmospheric structure and the circumstances that forced the atmospheric event along the Colombian coast and confirmed the location of a LLJ that drives the upwelling in the Guajira Peninsula. The air-sea energy transfers, ocean-surface distributions, and atmospheric structure displayed noticeable changes during

4 March to 9 April 2003, varying from normal to disrupted, with strong ocean-atmosphere conditions controlling the regional coastal upwelling. The impact of this event on the main ocean circulation features, the Caribbean Current, and the Panama-Colombia cyclonic gyre delimiting the upwelling pattern were evident in the ocean simulation.

[39] Some modifications are suggested for improving the data assimilation scheme. Since the system is operationally receiving United Kingdom Met Office's atmospheric data by coupling the ocean model to a higher resolution model outputs, it is possible to enhance the regional forecasting and climate variability description. Within this goal, it is recommended having an updated distribution of regional land surface characteristics and the inclusion of emission and transport physics of aerosols to investigate their potential effect on assimilated satellite surface temperature and influence on atmospheric radiative processes. Such model configuration will serve to develop scientific knowledge on different fronts encompassing regional investigations in weather and climate and studies on coastal,

oceanographic, land, and atmospheric environments with a focus on short- and long-term simulations.

[40] Analysis of longer simulations tracking the ocean-atmosphere interactions during winter–spring transitions is needed to analyze in detail the regional ocean-atmosphere climate variability. In addition, an in-depth model output and observational time series statistical analysis are required to conclusively demonstrate the newly described type of short-term (~days) variability affecting coastal upwelling in the region. Also, the seasonal variability needs to be analyzed to fully characterize the time scales of variability for the Guajira coastal upwelling. On the basis of our investigation for March 2003, the Guajira upwelling appears to respond to atmospheric forcing on two time scales of intra-annual variability: (1) the well-known seasonal modulation driven by the annual variation in trade wind intensity cited in the previous literature but so far not analyzed in depth and (2) short-term events, proposed in the present investigation, lasting a few days during the winter–spring transitional periods of the year. The disruption of upwelling occurs at the latter scale. These events, albeit short lived, are so strong that they can be comparable in intensity to the seasonal variations. It is clear that the anomalous events preferentially take place in spring and autumn, when the ITCZ is still in the Northern Hemisphere, while the midlatitude frontal system is still oscillating in the low-latitude areas.

[41] **Acknowledgments.** This research originally used computational resources, oceanographic instrumentation, and cruises supported by the Centro de Investigaciones Oceanográficas e Hidrográficas in Cartagena, Colombia. J. L. H. acknowledges support from Southeast Climate Consortium and Department of Agricultural and Biological Engineering at the University of Florida in the final data analysis and visualization presented in this investigation. D. M. P. was supported by funding from the Gordon and Betty Moore Foundation and NASA Applied Sciences Program, Earth Science Division, through a grant provided by Research Announcement NNH07ZDA001N, Research Opportunities in Space and Earth Sciences (ROSES-2007), Program Element A.20: Decision Support Through Earth Science Research Results. We thank Dr Arnold Gordon from Lamont-Doherty Earth Observatory and the anonymous reviewers for helpful comments on an earlier draft of this paper.

## References

- Andrade, C. A., and E. D. Barton (2005), The Guajira upwelling system, *Cont. Shelf Res.*, **25**, 1003–1022, doi:10.1016/j.csr.2004.12.012.
- Andrade, C. A., E. D. Barton, and C. N. K. Mooers (2003), Evidence for an eastward flow along the central and South American Caribbean coast, *J. Geophys. Res.*, **108**(C6), 3185, doi:10.1029/2002JC001549.
- Anduckia, J. C., and S. A. Lonin (2004), Efecto residual de la nubosidad en la asimilación de temperatura superficial del mar, *Boletín Científico CIOH*, **22**, 36–44.
- Blumberg, A. F., and G. L. Mellor (1987), A description of a three-dimensional coastal ocean circulation model, in *Three-Dimensional Ocean Coastal Models*, edited by N. S. Heaps, pp. 1–16, AGU, Washington, D.C.
- Carton, J. A., and Y. Chao (1999), Caribbean Sea eddies inferred from TOPEX/POSEIDON altimetry and a 1/6° Atlantic Ocean model simulation, *J. Geophys. Res.*, **104**(C4), 7743–7752, doi:10.1029/1998JC900081.
- Cayan, D. R. (1992), Variability of latent and sensible heat fluxes estimated using bulk formulae, *Atmos. Ocean*, **30**(1), 1–42.
- Centurioni, L. R., and P. P. Niiler (2003), On the surface currents of the Caribbean Sea, *Geophys. Res. Lett.*, **30**(6), 1279, doi:10.1029/2002GL016231.
- Conkright, M. E., R. A. Locarnini, H. E. Garcia, T. D. O'Brien, T. P. Boyer, C. Stephens, and J. I. Antonov (2002), *World Ocean Atlas 2001: Objective Analyses, Data Statistics, and Figures, CD-ROM Documentation*, 17 pp., National Oceanographic Data Center, Silver Spring, MD.
- Corredor, J. E. (1979), Phytoplankton response to low level nutrient enrichment through upwelling in the Columbian Caribbean Basin, *Deep-Sea Res.*, **26**(7A), 731–741, doi:10.1016/0198-0149(79)90010-4.
- Curl, H., Jr. (1960), Primary production measurements in the north coastal waters of South America, *Deep-Sea Res.*, **7**, 183–189, doi:10.1016/0146-6313(60)90024-1.
- da Silva, A., C. C. Young, and S. Levitus (1994), “Atlas of surface marine data 1994. Volume 1: Algorithms and procedures” Tech. Rep. 6, NOAA Natl. Environ. Sat., Data, and Inf. Serv., U.S. Dept. of Commerce, Washington, D. C.
- Dudhia, J. (1989), Numerical study of convection observed during the winter monsoon experiment using a mesoscale two-dimensional model, *J. Atmos. Sci.*, **46**, 3077–3107, doi:10.1175/1520-0469(1989)046<3077: NSOCOD>2.0.CO;2.
- Dudhia, J. (1993), A nonhydrostatic version of the Penn State-NCAR mesoscale model: Validation tests and simulations of an Atlantic cyclone and cold front, *Mon. Weather Rev.*, **121**, 1493–1513, doi:10.1175/1520-0493(1993)121<1493:ANVOTP>2.0.CO;2.
- Enriquez, A. G., and C. A. Friehe (1995), Effects of wind stress and wind stress curl variability on coastal upwelling, *J. Phys. Oceanogr.*, **25**, 1651–1671, doi:10.1175/1520-0485(1995)025<1651:EOWSAW>2.0.CO;2.
- Foltz, G. R., J. A. Carton, and E. P. Chassignet (2004), Tropical instabilities vortices in the Atlantic Ocean, *J. Geophys. Res.*, **109**, C03029, doi:10.1029/2003JC001942.
- Gordon, A. L. (1967), Circulation of the Caribbean Sea, *J. Geophys. Res.*, **72**, 6207–6223, doi:10.1029/JZ072i024p06207.
- Grell, G., and Y. Devenyi (2002), A generalized approach to parameterizing convection combining ensemble and data assimilation techniques, *Geophys. Res. Lett.*, **29**(14), 1693, doi:10.1029/2002GL015311.
- Hawkins, J. D., and D. W. Stuart (1980), Low-level atmospheric changes over Oregon's coastal upwelling region, *Mon. Weather Rev.*, **108**, 1029–1040, doi:10.1175/1520-0493(1980)108<1029:LLACOO>2.0.CO;2.
- Hernández, J., J. Srikishen, D. Erickson, R. Oglesby, and D. Irwin (2006), A regional climate study of central America using the MM5 modeling system: Results and comparison to observations, *Int. J. Climatol.*, **26**(15), 2161–2179, doi:10.1002/joc.1361.
- Hong, S.-Y., and H.-L. Pan (1996), Nonlocal boundary layer vertical diffusion in a medium-range forecast model, *Mon. Weather Rev.*, **124**, 2322–2339, doi:10.1175/1520-0493(1996)124<2322:NBLVDI>2.0.CO;2.
- Hunter, E., R. Chant, L. Bowers, S. Glenn, and J. Kohut (2007), Spatial and temporal variability of diurnal wind forcing in the coastal ocean, *Geophys. Res. Lett.*, **34**, L03607, doi:10.1029/2006GL028945.
- Kalnay, E., et al. (1996), The NCEP/NCAR 40-year reanalysis project, *Bull. Am. Meteorol. Soc.*, **77**(3), 437–471, doi:10.1175/1520-0477(1996)077<0437:TNYRP>2.0.CO;2.
- Kaufman, Y. J., I. Koren, L. A. Remer, D. Tanré, P. Ginoux, and S. Fan (2005), Dust transport and deposition observed from the Terra-Moderated Resolution Imaging Spectroradiometer (MODIS) spacecraft over the Atlantic Ocean, *J. Geophys. Res.*, **110**, D10S12, doi:10.1029/2003JD004436.
- Liu, W. T., W. Tang, and X. Xie (2008), Wind power distribution over the ocean, *Geophys. Res. Lett.*, **35**, L13808, doi:10.1029/2008GL034172.
- Lonin, S., J. C. Anduckia, C. Parra, and R. Molares (2003), *Modelo de circulación oceánica con asimilación de datos para el Caribe aplicado en derrames de hidrocarburos, pesquería y búsqueda y rescate. En el libro: Contribución en las Ciencias del Mar en Colombia*, pp. 103–120, Universidad Nacional de Colombia.
- Mooers, C. N. K., and G. A. Maul (1998), Intra-Americas Sea circulation, in *The Sea*, vol. II, edited by K. R. Brink and A. R. Robinson, pp. 183–208, Wiley, New York.
- Müller-Karger, F. E., and R. Aparicio (1994), Mesoscale Processes affecting phytoplankton abundance in the southern Caribbean Sea, *Cont. Shelf Res.*, **14**, 199–221, doi:10.1016/0278-4343(94)90013-2.
- Oey, L.-Y., H.-C. Lee, and W. Schmitz (2003), Effects of wind and Caribbean eddies on the frequency of loop current eddy shedding: A numerical model study, *J. Geophys. Res.*, **108**(C10), 3324, doi:10.1029/2002JC001698.
- Prospero, J. M., P. Ginoux, O. Torres, S. E. Nicholson, and T. E. Gill (2002), Environmental characterization of global sources of atmospheric soil dust identified with NIMBUS 7 Total Ozone Mapping Spectrometer (TOMS) absorbing aerosol product, *Rev. Geophys.*, **40**(1), 1002, doi:10.1029/2000RG000095.
- Richards, F. A. (1960), Some chemical and hydrographic observations along the north coast of South America: I. Cabo Tres Puntas to Curacao, including the Cariaco Trench and the Gulf of Cariaco, *Deep Sea Res.*, **7**, 163–182, doi:10.1016/0146-6313(60)90023-X.
- Richardson, P. L. (2005), Caribbean Current and eddies as observed by surface drifters, *Deep Sea Res., Part II*, **52**, 429–463, doi:10.1016/j.dsr2.2004.11.001.

- Shultz, D. M., W. E. Bracken, and L. F. Bosart (1998), Planetary- and synoptic-scale signatures associated with central American cold surges, *Mon. Weather Rev.*, *126*, 5–27, doi:10.1175/1520-0493(1998)126<0005:PASSSA>2.0.CO;2.
- Vernekar, A. D., B. P. Kirtman, and M. J. Fennesy (2003), Low-level jets and their effects on the South American summer climate as simulated by the NCEP eta model, *J. Clim.*, *16*, 297–311 doi:10.1175/1520-0442(2003)016<0297:LLJATE>2.0.CO;2.
- Wüst, G. (1964), *Stratification and Circulation in the Antillean-Caribbean Basins*, 201 pp., Columbia Univ. Press, NY.
- Xu, H., S.-P. Xie, Y. Wang, and R. J. Small (2005), Effects of central American mountains on the eastern Pacific winter ITCZ and moisture transport, *J. Clim.*, *18*, 3856–3873, doi:10.1175/JCLI3497.1.
- 
- J. L. Hernández, Agricultural and Biological Engineering Department, University of Florida, Frazier Roger Hall, Ofc. 256, Gainesville, FL 32611, USA. (jose.l.hernandez@ufl.edu)
- S. A. Lonin, Facultad de Oceanografía Física, Escuela Naval de Cadetes “Almirante Padilla,” Cartagena, Colombia.
- D. M. Palacios, Joint Institute for Marine and Atmospheric Research, University of Hawaii at Manoa, 1000 Pope Road, Marine Science Building 312, Honolulu, HI 96822, USA.